Polyoxazoline hydrogels fabricated by stereolithography

Thomas Brossier, Belkacem Tarek Benkhaled, Maxime Colpaert, Gael Volpi, Olivier Guillaume, Sébastien Blanquer, Vincent Lapinte

Polyoxazoline hydrogels fabricated by stereolithography†

Thomas Brossier,[a,b] Belkacem Tarek Benkhaled,[a] Maxime Colpaert,[a] Gael Volpi,[b] Olivier Guillaume,[c] Sébastien Blanquer*[a] and Vincent Lapinte*[a]

The development of hydrogel materials in additive manufacturing displaying stiff and strong mechanical properties while maintaining high water uptake remains a great challenge. Taking advantage of the versatility of poly(oxazoline) (POx) chemistry and properties, we investigated in this article a new generation of POx hydrogels fabricated by stereolithography (SLA). A large range of photosensitive poly(2-methyl-2-oxazoline) resins were synthesized as hydrogel precursors for SLA photofabrication. Functionalization has been performed by direct di-methacrylation of POx terminal groups (MA_2POx_n) or by multi-methacrylation of poly(ethyleneimine) (PEI) units resulting from partial POx hydrolysis (MA_mPOx_n–PEI_p). The length and the functionality of these UV-active macro-crosslinkers influence both the mechanical properties and the hydration behavior of the resulting hydrogels. The benefit of the layer-by-layer crosslinking of the POx resin during the vat photopolymerization allowed the fabrication of complex and well-defined 3D objects. The high-definition and high mechanical strength of these copolymers allow the fabrication of stiff and strong 3D hydrogels. The cytocompatibility test of the POx derivatives was conducted in solution and once the cells are encapsulated within 3D hydrogels. Finally, porous 3D scaffolds with gyroid architectures were built which provide opportunities for POx materials in tissue engineering applications.

Received 26th January 2022,
Accepted 1st April 2022

Introduction

Hydrogels are soft three-dimensional hydrophilic networks able to absorb a large quantity of water without losing their mechanical integrity.[1–3] The large hydration contributes not only to a certain biocompatibility, but also allows them to get closer to the chemical and physical structures of biological tissue.[1,3,4] Therefore, hydrogels are extremely suitable for a variety of applications in the pharmaceutical and medical industry and more particularly in tissue engineering.[3,5]

However, hydrogels are also widely known for their weakness and low elasticity which then limit their use in applications where mechanical solicitations are expected.[6] One of the options to reinforce the mechanical resistance of hydrogels is using synthetic polymers. Hydrogels based on synthetic polymers have often been employed because of their tunable, controllable and reproducible properties (chemistry, structure, porosity, degradability *etc.*).[7,8] Such versatility of properties is even more beneficial in additive manufacturing and precisely in the vat photopolymerization process.[9] In fact, the layer-by-layer photo-curing process overcomes the limited crosslinking depth resulting from bulk irradiation, due to issues of light absorption and diffusion in thick samples. Moreover, vat photopolymerization such as stereolithography (SLA) offers a unique path that allows not only precise control of the external architecture of three-dimensional objects, but also the ability to produce highly sophisticated porous structures which is a huge benefit for tissue engineering scaffolds.[10]

Poly(ethylene glycol) (PEG) is recognized to be the gold standard of hydrophilic synthetic polymers in the biomedical field, and consequently has been widely used in SLA to build hydrogels.[10] Methacrylated PEG and its derivatives were proposed as precursor resins for SLA fabrication, especially for tissue engineering application.[11] Unfortunately, PEG was proved to generate an immune response[12] and it accumulates in the body tissues due to its biostability,[13,14] which then explains the need to find an alternative.

Among all the hydrophilic synthetic polymers, the polyoxazoline (POx) family seems to avoid this phenomenon, as shown by Zalipsky *et al.*, which is a reason for its considerable growing representation in the literature.[15] Moreover, hydrogels based on PEG usually suffer from brittleness and low water uptake for short chains, or low strength for long chains.[16] Consequently, we aim to produce POx hydrogels with high water uptake while keeping the physical integrity under load,

[a]*ICGM, University of Montpellier, CNRS, ENSCM, Montpellier, France. E-mail: vincent.lapinte@umontpellier.fr*
[b]*3D Medlab, Marignane, France*
[c]*3D Printing and Biofabrication Group, Institute of Materials Science and Technology, TU Wien, Getreidemarkt 9/308, 1060 Vienna, Austria*
†Electronic supplementary information (ESI) available. See DOI: https://doi.org/10.1039/d2bm00138a

characterized by a high elastic modulus and fracture strength. POx is qualified as a pseudo-peptide and synthesized by living cationic ring-opening polymerization (CROP) of commercial 2-R-2-oxazoline monomers where R corresponds to alkyl or aromatic groups. The well-known candidates amongst the members of the POx family are poly(2-methyl-2-oxazoline) (PMOx) and poly(2-ethyl-2-oxazoline) (PEtOx). These polymers are considered as promising water-soluble polymers, exhibiting a low degree of toxicity,[17] largely employed in the health field[18,19] and appearing as a legitimate substitute for PEG.[20–22] POx are easily tunable with manifold end-groups and offer an additional ability to be partially or fully hydrolysed into poly (ethyleneimine), leading to POx-PEI or PEI, respectively.[23–25] This modification opens the door to another generation of grafted polymers which correspond to POx substituted by functional pendent chains[26] as already reported for photosensitive methacrylate groups by the Hoogenboom[27] and Schubert[28] teams and our team with coumarin units.[29–31] Nevertheless, to the best of our knowledge, the use of photosensitive POx resin has never been reported for SLA, even though the POx hydrogel was very recently reported as a polymer precursor for other additive manufacturing processes.[32] Luxenhofer *et al.* studied biomaterial inks based on thermoresponsive PMOx-*b*-PPheOzi-*b*-PMOx[33] or PMOx-*b*-PnPOx[34] alone or combined with nanoclay LAPONITE® XLG[35–37] in extrusion-based 3D printing. The bioprinting approach relies on the thermogelling properties of precursors, and consequently does not require the photo-reactive POx resin. Finally, Schubert *et al.* described 3D microstructures produced using two-photon polymerization by mixing different chain lengths of photo-sensitive poly(2-ethyl-2-oxazoline).[38]

Herein, we investigated photo-sensitive poly(2-methyl-2-oxazoline) in the SLA process. Di- and multifunctional POx precursors were synthesized by methacrylation of either terminal end groups of POx or lateral ethyleneimine units of POx–PEI resulting from the partial hydrolysis of POx (Fig. 1). Independent of additive manufacturing, special attention was given on the physical and mechanical properties of the POx hydrogels, which have been barely reported in the literature. These tailor-made polymers used as photo-crosslinkable resins in SLA allowed fabricating well-defined 3D objects as the Paris triumphal arch or structures with gyroid porous architectures with great potential to be used as scaffolds for tissue engineering.

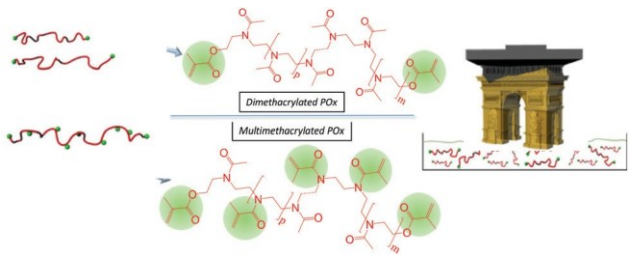

Fig. 1 Methacrylated POx hydrogels using the stereolithography process.

Materials and methods

Materials

2-Methyl-2-oxazoline (MOx, Sigma Aldrich, 99.0%), 1,6-hexanediol (HD, Sigma Aldrich, 99.0%), methyl *p*-toluene sulfonate (MeOTs, Sigma Aldrich, 97.0%), methacrylic acid (MAA, Alfa Aesar, 99.0%), triethylamine (TEA, Sigma Aldrich, 98.0%), anhydrous acetonitrile (Sigma Aldrich, 99.9%), *p*-toluenesulfonyl chloride (TsCl, Sigma Aldrich, 99.0%), methacrylic anhydride (Sigma Aldrich, 94%), orange G (Sigma Aldrich), potassium hydroxide (Sigma Aldrich, 90%), and diethyl ether were commercial products and used without further purification. Liquid TPO was acquired from BASF (Germany). Dialysis membranes, Spectra/Pors-MWCO 1.5 kDa, were purchased from Spectrum Laboratories.

Synthesis

Synthesis of 1,6-hexaneditosylate (HDOTs). To a 250 mL round-bottom flask equipped with a magnetic stir bar, 1,6-hexanediol (HD) (10 g, 0.85 mol) and TEA (57 mL, 4.25 mol) were dissolved in 100 mL of chloroform. The solution was cooled at 0 °C and TsCl (65 g, 3.4 mol) was added dropwise. The resulting mixture was stirred overnight at 25 °C. The crude product was washed with water and 3 times with dichloromethane. The organic phase was concentrated and stored in a fridge until crystallization. The compound was recrystallized with ethanol and a white solid product was isolated in 75% yield.

^{1}H NMR ($CDCl_3$), δ (ppm): 7.7 (d, 4H, Hd), 7.3 (d, 4H, Hc), 3.9 (t, 4H, Hb), 2.5 (s, 6H, He), 1.6–1.3 (m, 8H, Ha) (Fig. S1†).

Synthesis of bis-methacrylated poly(2-methyl-2-oxazoline) (M_2POx_n). To a 500 mL round-bottom flask equipped with a magnetic stir bar, HDOTs (11 g, 0.029 mol) was dissolved in 300 mL of anhydrous acetonitrile and MOx (49.5 mL, 0.588 mol) were added. The solution was vigorously stirred at 80 °C for 4 h. The resulting polymer was then quenched by the dropwise addition of TEA (27 mL, 0.196 mol) and methacrylic acid (13 ml, 0.714 mol). The flask was maintained at 40 °C for 15 h. After cooling, the reaction mixture was concentrated, then precipitated in diethyl ether and dried under pressure. A solid powder was obtained with a yield of 93%.

^{1}H NMR ($CDCl_3$) δ (ppm): 6.08 (1H, He1), 5.26 (1H, He2), 4.28 (2H, Hc) 3.20–3.66 (4H, Hb), 1.96–2.19 (3H, Hd), 1.94 (3H, Hf), 1.06–1.59 (8H, Ha) (Fig. S2†).

Synthesis of monomethacrylated poly(2-methyl-2-oxazoline) ($MPOx_n$). To a 500 mL round-bottom flask equipped with a magnetic stir bar, MeOTs (9.1 g, 0.049 mol) was dissolved in 300 mL of anhydrous acetonitrile and MOx (49.5 mL, 0.588 mol) were added. The solution was vigorously stirred at 80 °C for 4 h. The resulting polymer was then quenched by the quick addition of a solution of methacrylic acid (12.5 mL, 0.147 mol) and triethylamine (27.3 mL, 0.196 mol). The flask was maintained at 40 °C for 15 h. After cooling, the reaction mixture was concentrated, then precipitated in diethyl ether and dried under a vacuum pump. A sticky solid was obtained with a yield of 95%.

^{1}H NMR ($CDCl_3$) δ (ppm): 6.0 (1H, He1), 5.5 (1H, He2), 4.15 (2H, Hd), 3.1–3.6 (4H, Hb), 2.9 (3H, Ha), 1.9–2.1 (3H, Hc), 1.8 (3H, Hf) (Fig. S3†).

Synthesis of methacrylated poly(2-methyl-2-oxazoline) (PEI) (MA_oPOx_m–$PEI_{p'}$). Step 1. Ring-opening polymerization of MeOx (DP_n = 100) (POx_n)

To a 500 mL round-bottom flask equipped with a magnetic stir bar, HDOTs (2.51 g, 5.8 mmol) was dissolved in 90 mL of anhydrous acetonitrile and MOx (49.5 g, 588 mmol) were added. The solution was vigorously stirred at 80 °C for 24 h. Then, the growing polymer chains were quenched at 40 °C by addition of an adequate amount of methanolic potassium hydroxide solution (50 mL at 2 M). The flask was maintained at 40 °C overnight. After cooling, the reaction mixture was concentrated and after precipitation in cold diethyl ether a resulting POx_n was dissolved in water (100 mL) and freeze-dried into a dry white powder (45 g, 90% yield).

^{1}H NMR ($CDCl_3$) δ (ppm): 3.20–3.66 (4H, Hb), 1.96–2.19 (3H, Hc), 1.06–1.59 (8H, Ha) (Fig. S4†).

Step 2. Partial hydrolysis of POx_n into POx_m–PEI_p

A 6 M HCl solution was prepared from distillated water (100 mL) and hydrochloric acid solution 37% (150 mL). POx_n (40 g) was dissolved in the previous solution. The round-bottom flask was heated at 100 °C. After 1.5 h of hydrolysis roughly 40% of *N*-acylmethylene imine repetitive units were converted into the corresponding ethylene imine moieties (EI). The mixture was cooled until room temperature, and then a concentrated NaOH solution 2.5 M was added to neutralize the mixture at pH = 7. The propionic acid by-product was removed by dialysis using a 1 kDa dialysis membrane over 48 h. The water was removed by freeze-drying to obtain a powder in a good yield (29 g, 72.5%). The hydrolysis rate (*H*%) was calculated by ^{1}H NMR spectroscopy using the integration of the corresponding peak of the NCH_2CH_2 protons of POx_n related to that of PEI using eqn (1):

$$H\% = \frac{\int CH\ PMOx}{\int CH_2PEI} \times 100 \quad (1)$$

^{1}H NMR ($CDCl_3$) δ (ppm): 3.20–3.66 (4H, Hb), 2.57–2.84 (4H, Hc), 1.96–2.19 (3H, Hd), 1.06–1.59 (8H, Ha) (Fig. S5†).

Step 3. Methacrylation of POx_m–PEI_p into MA_oPOx_m–$PEI_{p'}$

POx_m–PEI_p (19 g, 2.23 mmol) was dissolved in anhydrous dichloromethane. A solution of anhydride methacrylic (6.99 mL, 46 mmol) and TEA (15.65 mL, 112.5 mmol) in anhydrous dichloromethane (10 mL) was added dropwise to the initial solution. Then, the mixture was maintained at room temperature for 3 days. After that, the reaction mixture was concentrated, then precipitated in diethyl ether and dried under pressure. Finally, the resulting polymer was dissolved in water (100 mL) and freeze-dried. A solid powder was obtained in a good yield (16.5 g, 86%).

^{1}H NMR ($CDCl_3$) δ (ppm): 6.01 and 5.5 (2H, Hh), 4.93–5.27 (2H, Hf), 3.20–4.2 (4H, Hb), 2.4–2.7 (4H, Hc), 1.98–2.19 (3H, He), 1.96 (3H, Hg and 3H, Hi), 1.06–1.59 (8H, Ha) (Fig. S6†).

Characterization of the methacrylated POx resins

Nuclear magnetic resonance (NMR). ^{1}H NMR spectra were recorded on a 400 MHz Bruker Aspect Spectrometer. D_2O was used as a deuterated solvent. Chemical shifts were given in parts per million (ppm). For ^{1}H NMR the residual H_2O and $CHCl_3$ in D_2O and $CDCl_3$ at 4.79 and 7.26 ppm was considered as the reference peaks. The molar mass of MA_2POx_n was determined using the following eqn (2) and (3):

$$DP_{n,MA_2POx} = \frac{\frac{\int_{3.8}^{3.2} I}{8}}{\frac{\int_{6.1}^{5.7} I}{4}} \quad (2)$$

$$M_{n,NMR} = DP_n \times M_{MOx} + 2M_{methacrylate} \quad (3)$$

where M_{MOx} and $M_{methacrylate}$ are the molar masses of the MOx repetitive unit (85 g mol^{-1}) and the methacrylate end chain (86 g mol^{-1}), respectively.

Size exclusion chromatography (SEC). The apparent number-average molar masses and dispersity of MA_nPOx were determined using a *N*,*N*-dimethylacetamide (DMAc) GPC system (PL-GPC 50 Plus) equipped with an autosampler (Varian model 410). The SEC apparatus comprised a refractive index detector and was filled with one PolarGel-M pre-column (7.5 × 50 mm) and two PolarGel-M columns (7.5 × 300 mm) thermostated at 50 °C. The mobile phase was DMAc (with 0.1 wt% LiCl) at a flow rate of 0.8 mL min^{-1}, calibrated with poly(methylmethacrylate) (PMMA) standards ranging from 550 to 2 000 000 g mol^{-1} (EasiVial-Agilent).

Viscosimetry. The viscosity of the POx based resins was determined by rheological measurements using a Physica Modular Compact MCR301 Rheometer from Anton Paar (Germany) and a parallel plate model. The viscosity of the POx resin was determined by oscillatory measurements over time at 30 s^{-1} shear rate at 25 °C.

Fabrication of 3D printed objects by SLA using MA_2POx_n resins

The 3-D porous scaffolds were designed using the STL format from K3DSurf and Rhinoceros 3D. Gyroid structures were produced from eqn (4):[39]

$$\cos(x) \cdot \sin(y) + \cos(y) \cdot \sin(z) + \cos(z) \cdot \sin(x) = 0.75 \quad (4)$$

POx based macromonomers (MA_oPOx_m–$PEI_{p'}$ or $MAPOx_n$/MA_2POx_n blend) were dissolved in distilled water at a concentration ranging from 40 to 60 wt% depending on the length of POx and stirred until fully dissolved. Liquid TPO (3% w/w) photoinitiator and Orange G (0.2% w/w) photoabsorber were added to the POx solution and stirred for a few minutes to allow homogeneous photopolymerization and provided an efficient cure depth and optimal pattern resolution.

The ideal layer thickness was fixed at 100 μm. The optimal layer thickness was determined using Jacob's equation.[40] Briefly, 6 drops of formulated resin were placed successively on a transparent plate and irradiated at 20 mW cm^{-2} for 10, 20, 30, 40, 50, and 60 s. Then, the glass plate was carefully wiped to remove all the unpolymerized material. A digital thickness gauge (Schmidt, Germany) was used to measure the cure depth with 10 μm precision.

The 3D structures were then built from the above-mentioned resins by SLA using 385 nm digital light processing (DLP) apparatus (Asiga Max X27, Australia). The 3D objects were constructed by photo-crosslinking layer-by-layer with a thickness of 100 μm, selected from the above-mentioned test. Each layer was illuminated over an intensity of 20 mW cm^{-2} with different irradiation times (Table SI7†). After building, the scaffolds were removed from the stage and washed using distilled water to remove unreacted prepolymer residues from the scaffolds.

Characterization of the 3D printed hydrogels

Mechanical testing. Compression tests of hydrogels were realized on an Instron 3366L5885 mechanical tester. Cylindrical samples of 10 × 5 mm were prepared by SLA and poured onto water for 2 days before the test. The compression stress test was operated at a rate of 5 mm s^{-1}. The compression strain was expressed as a percentage of the original length. Each point represented the mean ± SD (n = 3).

Scanning electron microscopy (SEM). The hydrogels were freeze-dried and sputter-coated with gold before being photographed using a scanning electron microscope (SEM) (Phenom-world ProX) with an accelerating voltage of 10 kV.

Network studies. The water uptake of hydrogels was calculated from the swollen weight (w_s) and the dry weight (w_d). Freshly prepared hydrogels were weighed after irradiation to obtain m_i and kept in distilled water for 48 h (water renewed five times). After swelling, the hydrogels were weighed to determine w_s and vacuum-dried to deduce w_d. The crosslinking efficiency was calculated using the gel content (eqn (5)) and the water absorption was determined from the equilibrium water uptake (Q) (eqn (6)):

$$\text{gel content} = \frac{w_s}{w_d} \times 100 \quad (5)$$

$$Q = \frac{w_s - w_d}{w} \times 100: \quad (6)$$

The average molar mass between cross-links ($\overline{M_c}$) is estimated from the equilibrium swelling theory using eqn (7):

$$\overline{M_c} = -V_1 \rho_p \frac{\xi^{1/3} - \frac{V_s}{2}}{\ln(1 - V_s) + V_s + \chi V_s^2} \quad (7)$$

where V_1 is the molar volume of water (18 cm^3 mol^{-1}), ρ_p and ρ_s are the polymer density and the solvent density estimated to be 1.14 and 1.00 g mL^{-1} respectively and χ is the Flory–Huggins interaction parameter between the solvent and polymer (χ = 0.06) according to the Van Krevelen calculation (δ_{PMOx} = 24.61 (cal $cm^{-3})^{1/2}$ and δ_{water} = 23.2 (cal $cm^{-3})^{1/2}$).

V_s is the volume fraction of the polymer in the swollen gel corresponding to eqn (8):

$$V_s = \left(1 + \frac{\rho_p}{\rho_s} \cdot \frac{w_s}{w_d} - 1\right)^{-1} \quad (8)$$

The mesh size of a swollen polymeric network (ξ) is defined as the linear distance between two adjacent crosslinks and is a key structural parameter for hydrogels. The mesh size ξ can be calculated using eqn (9) according to equilibrium swelling theory:

$$\xi(Å) = \left(\frac{2C_n M_c}{M}\right)^{1/2} l V_s^{-1/3} \quad (9)$$

where l is the carbon–carbon bond length (1.54 Å) and C_n is the value of the Flory characteristic ratio which was considered as that of poly(*N*-vinylpyrrolidone), 9.76, as previously reported by Hoogenboom.[41]

Cross-link density (q) is one of the most significant structural parameters for a family of hydrogels which influences the water absorbency (eqn (10)).

$$q = M_o / M_c \quad (10)$$

where M_o is the average molecular mass of the repetitive unit of the polymer (85 g mol^{-1} for poly(2-methyl-2-oxazoline)).

Cytocompatibility evaluation of the hydrogels as bioinks

Cytocompatibility protocol for soluble POx resin precursors. The different polymers were dissolved in a medium consisting of DMEM-HG supplemented with 1% P/S and 10% serum, at 2.5, 5, 10 and 20% (w/v).

The L929 fibroblasts (murine fibroblast cell line (purchased from Sigma-Aldrich), routinely used for assessing the cytocompatibility) were seeded at a density of 5.0 × 10^3 cells per well in 96-well plates and cultivated for two days. Next, the culture medium was removed and the cells were incubated in 200 μL of the extracts (n = 6 per condition). Extract-free HG-DMEM was applied as the feeding medium for the cells as positive controls, whereas the culture medium supplemented with 5% DMSO was applied as the feeding medium for the cells as a negative control. After 48 hours, the metabolic activity of the L929 fibroblasts was assessed using the PrestoBlue™ cell viability reagent (Invitrogen, Fisher Scientific, Vienna, Austria) according to the recommendation of the supplier. The morphology of the cells spreading onto the plastic of the 96 wp was also observed by taking images after the extract test, using bright field imaging of the LSM700 (Zeiss, Germany), mag. 20, Camera AxioCam 105.

Cytocompatiblity protocol of the embedded cells in POx hydrogels. Following the cytocompatibility test of the soluble polymers, we conducted a cytocompatibility test directly on cells embedded within the photo-crosslinked gels. For this experiment, another cell line was selected, immortalized human adipose-derived mesenchymal stem cells (hASC/hTERT) (Evercyte, Austria), which offers better interest for tissue engineering than the previously used cell line L929. The hASCs were expanded using EGM-2 BulletKit™ medium (Lonza, Switzerland) supplemented with 10% (v/v) newborn calf serum (NBCS) (Gibco, New Zealand) and maintained under standard culturing conditions (37 °C, 5% CO_2, humidified atmosphere). For the embedding experiment, hASCs passage 8, at a final concentration of 0.5.10^6 cells per mL within the gels were used. The final polymer concentrations

for the gels were fixed at 20 and 50 wt%, and contained 0.6 mM photoinitiator [lithium (2,4,6-trimethylbenzoyl)-phenylphosphinate] (Li-TPO) as the photo-initiator. After mixing all the components in fully supplemented EGM-2, drops of 20 µL (containing 10 000 hASCs) were cast onto each well of a 48-well plate and irradiated using a UV-chamber ((LITE-Box G136 368 nm; NK-OPTIK, Germany) for 5 min to induce hydrogel cross-linking (1 J). Following photo cross-linking, the wells were filled up with 500 µL of medium and kept in culture until analysis. The viability of the cells was determined by a Live/Dead® assay (Invitrogen, OR) using 0.2 µM calcein-AM (live stain) and 0.6 µM propidium iodide (dead stain) in a serum-free medium for 60 min at 37° C. The viability of cells was monitored on day 3 and day 7, using a confocal laser scanning microscope LSM 700 (Zeiss, Germany). The amount of viable (green cells) and dead (red cells) cells were counted on 6 images taken on 2 different samples per group. In addition, a metabolic test (PrestoBlue™ Cell Viability) was also performed 3 days post-encapsulation as previously described.

Results and discussion

Considering the limited number of synthetic hydrogels fabricated by SLA, we propose in this article to study a series of hydrosoluble photo-sensitive POx resins with different molecular weights and methacrylated rates to produce well-defined 3D hydrogels by SLA.

Consequently, two structures of photo-sensitive POx precursors of hydrogels are considered: α,ω-methacrylate POx (MA_2POx_n, route 1) and the more sophisticated macromolecular architecture bearing supplementary pendant methacrylate groups along the polymer chain to yield a higher functionality (MA_oPOx_m–$PEI_{p'}$, route 2) (Fig. 2A). In the first case, MA_2POx_n were produced in a one pot strategy based on the cationic ring-opening polymerization (CROP) of 2-methyl-2-oxazoline (MOx) using the 1,6-hexaneditosylate (HDOTs) initiator followed by *in situ* terminal methacrylation in the presence of methacrylic acid. The initial monomer/initiator ratio provides various lengths of the POx chain ranging from 1 to 10 kg mol^{-1} (eqn (3)) corresponding to a degree of polymerization average number (DP_n) of 10 and 120 respectively, as summarized in Table 1. The DP_n values were calculated by ^{1}H NMR spectroscopy by integration of the corresponding signals of POx ethylene (3.5 ppm) or methyl (2.0 ppm) protons related to initiator ones at 1.0 ppm according to eqn (2). SEC analysis depicted well-defined oligomers with a single population and a low dispersity of around 1.2–1.3 (Fig. 2B and Table S1†).

Route 2 employs the same CROP initiator HDOTs with potash as the terminating agent to afford α,ω-hydroxy POx (POx_n) before partially hydrolyzing *N*-acylethylene units of POx into ethylene units (POx_m–PEI_p) under acidic conditions (HCl) as previously described.[25] The ratio of hydrolysis is estimated from the ethylene signal at 2.6–2.8 ppm, providing a 40% conversion of the 110 initial units giving POx_{66}–PEI_{44} (Fig. 2C). The next step consists of the methacrylation of the amine

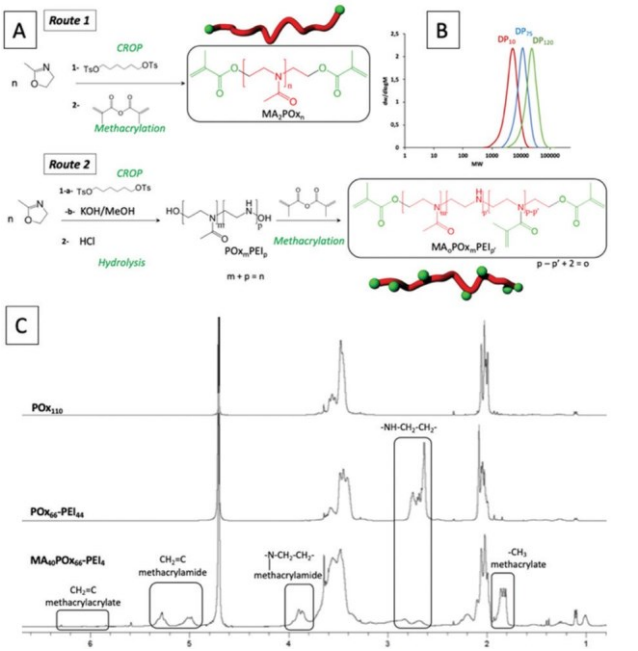

Fig. 2 (A) Synthetic routes to hydrogel precursors: MA_2POx_n and $MA_oPOx_mPEI_{p'}$. (B) GPC traces in DMAc of MA_2POx_n. (C) ^{1}H NMR spectra of $PMOx_{110}$, POx_{66}–PEI_{44}, and $MA_{40}POx_{66}$–PEI_4 (D_2O).

Table 1 Characteristics of POx precursors

Name	Units of POx//PEI/MA[a]	F[b]	M_n[a,c] (g mol^{-1})	MEW[d] (g mol^{-1})
MA_2POx_{10}	10/0/2	2	1080	540
MA_2POx_{75}	75/0/2	2	6605	3302
MA_2POx_{120}	120/0/2	2	10 430	5215
$MA_{40}POx_{66}$–PEI_4	66/4/40	40	10 252	285

[a] Values calculated by ^{1}H NMR spectroscopy. [b] Functionality of the oligomer POx in methacrylate units. [c] $M_n = DP_{n,\ POx} \times 85 + DP_{n,\ PEI} \times 44 + F \times 68 + Ext$. [d] Methacrylate-equivalent weight.

located along the POx_m–PEI_p chain as well as the terminal hydroxy groups. In the ^{1}H NMR spectrum, the ethylenic protons of methacrylate (5.8–6.3 ppm) were easily distinguished from those of methacrylamide (4.9–5.3 ppm) in Fig. 2C. We also noted the unreacted PEI units at 2.6–2.8 ppm resulting in $MA_{40}POx_{66}$–PEI_4.

The methacrylate equivalent weight (MEW) parameter in Table 1 is calculated from the molecular weight and the functionality of the POx precursors. This parameter shows the obvious increase of MEW value with the molecular weight of the MA_2POx_n series. Moreover, the low MEW value of $MA_{40}POx_{66}$–PEI_4 *versus* MA_2POx_n illustrates a higher density of methacrylate for the MA_2POx_n series.

Study of POx hydrogels manufactured by stereolithography

The investigated hydrogel samples based on MA_2POx_n and $MA_{40}POx_{66}$–PEI_4 were fabricated by SLA. We noted the high-water solubility of the POx precursors allowing additive manu-

facturing in water which can be an advantage for applications involving biological substances unstable in organic solvents or even with cells. In order to settle the conditions of processability, the viscosity of the POx resins was targeted to be lower than 1 Pa s (Fig. S7†). Consequently, the POx precursors were more or less diluted in terms of their chemical architectures (polymer length and methacrylate functionality) as listed in Table S2.† Other machine parameters were optimized as well as the amount of photoabsorbent (Orange G) and the curing time to improve the layer-by-layer resolution.

To study the mechanical properties of the hydrogels based on MA_2POx_n and $MA_{40}POx_{66}$–PEI_4, cylinder shapes were fabricated by SLA and examined under compression. From the compression test curves (Fig. 3C), the Young's modulus (E) in the low strain region and the stress (σ_{max}) and the strain (ε_{max}) at break were deduced and are reported in Fig. 3A and B. As expected, E and σ_{max} decreased with the length of MA_2POx_n while ε_{max} increased from 22 to 48%. It has to be noted the remarkable high modulus values for the produced hydrogels, ranging here from 0.79 to 4.33 MPa. However, hydrogels based on $MA_{40}POx_{66}$–PEI_4 displayed unexpectedly high strain with a low elastic modulus. In fact, theoretically such chemical configurations should increase the number of crosslinking nodes which then must lead to a dense and rigid material. Such behavior can be hypothetically explained by the non-participation of some methacrylate units in network building due to their intramolecular reactions along the same chain forming bridges without reducing the network size.

In an additional study, a bicomponent resin made of a blend of MA_2POx_{10} with monomethacrylated POx ($MAPOx_{10}$) (0.1% w/w) was also considered in order to enhance the elongation of the hydrogels (Table S3†). The logical decrease of the Young's modulus (0.159 MPa) for a lower network density was observed, whereas ε_{max} (27.4%) and σ_{max} (0.063 MPa) did not change (Fig. 3A). Thus, the single component resins (MA_2POx_n or $MA_{40}POx_{66}$–PEI_4) where the reactant reacts with itself own more attractive mechanical properties compared to the bicomponent resin.

For all the POx hydrogels, the equilibrium water uptake (Q) and gel content were calculated according to eqn (5) and (6) and are summarized in Fig. 3A. Other network parameters including the average molar mass between crosslinks ($\overline{M}_c$), the crosslink density (q) (Table S4†) and finally the mesh size (ξ) (Fig. 3A and D) of the photo-crosslinked materials can be deduced from the equilibrium swelling theory.

It must be noted that the water uptake for all the POx hydrogels was extremely high, even for the smaller precursor, MA_2POx_{10}, with 186% of water content which is nonetheless associated with the network with the lowest mesh size. The water uptake, the mesh size (ξ), and consequently $\overline{M}_c$ increase with the DP_n, inversely to the elastic modulus (Fig. 3B). This behavior is typically due to the reduction of the network density when DP_n is increasing. We noted that the ξ values are slightly higher than those of other POx hydrogels described by Hoogenboom *et al.* (10–130 nm).[41] Such impressive water uptake of MA_2POx_n is hardly observed with other synthetic hydrogels. In comparison to PEG hydrogels, POx hydrogels interestingly display both a high Young modulus and high water uptake. Smith Callahan *et al.* used hydrogels with a similar length chain of dimethacrylated PEG (8 kDa) and measured a close Young modulus of 3.8 MPa and only a swelling ratio of 22% (ξ of 6–9 nm).[42] The higher water uptake of POx *versus* PEG hydrogel can be justified by the higher hydrophilic character of PMOx as previously reported.[43,44] Despite the numerous POx-based hydrogels reported in the review of Wiesbrock *et al.* only a few of them reported on their mechanical properties.[45] Kronek *et al.* described hydrogels of poly(2-butenyl-2-oxazoline) photo-crosslinked by thiol–ene coupling using various dithiol crosslinkers with a similar water uptake of 600% and a Young's modulus of 1 MPa.[46]

Of note is the surprising high water uptake, of around 650%, for $MA_{40}POx_{66}$–PEI_4, characteristic of a wide network whereas we expected to generate a denser one due to the numerous methacrylate/methacrylamide units per chain (Fig. 3A). This confirms the hypothesis of intramolecular crosslinking between methacrylamides present along the same chain.

To illustrate the swelling ability of POx-based resins, the logo of our institute "ICGM plate" model was fabricated by SLA with the MA_2POx_{10} resin and incubated in water for 24 hours (Fig. 3D). From the picture, we can easily identify the swelling effect upon hydration of the hydrogel, but still maintaining the initial high resolution.

A

Name	E^a (MPa)	$\sigma_{max}{}^a$ (MPa)	$\varepsilon_{max}{}^a$ (%)	Gel content^b (%)	Q^c (%)	ξ^d (nm)
MA_2POx_{10}	4.33	1.61	22	75	186	177
MA_2POx_{75}	2.03	1.15	31	78	298	263
MA_2POx_{120}	0.79	1.26	48	98	573	524
$MA_{40}POx_{66}$-PEI_4	0.15	0.25	60	85	655	-^{e}

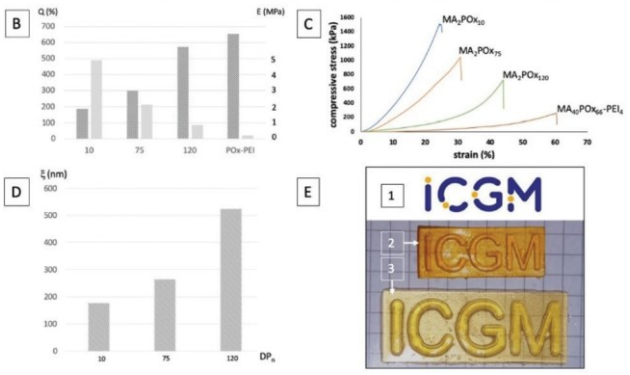

Fig. 3 (A) Mechanical and water uptake of POx hydrogels fabricated by SLA. [a] Deducted from the mechanical curve. [b] Calculated with eqn (5). [c] Calculated with eqn (6). [d] Calculated with eqn (9). [e]Not determined. (B) Equilibrium water uptake (Q) (dark grey) and Young's modulus (light grey) related to the length of the POx chain of MA_2POx_n and $MA_{40}POx_{66}$–PEI_4. (C) Compressive stress related to the strain of MA_2POx_n and $MA_{40}POx_{66}$–PEI_4. (D) The mesh size of MA_2POx_n hydrogels related to the length of the POx chain. (E) Illustration of the swelling of the POx-based resin (*e.g.* MA_2POx_{10}) with the ICGM plate logo of the Institute Charles Gerhardt of Montpellier ((1) original logo, (2) plate bearing ICGM logo fabricated by SLA and (3) the same plate in the swollen state).

To highlight the potential to manufacture sophisticated structures by SLA with POx-based resins, the triumphal arch of Paris was designed and fabricated. The monument is typically constituted of two higher arches in face and two smaller side arches supported by four pillars. Such an architectural configuration is not only challenging in terms of fabrication due to the over-hanging design, but also for the stability of the system based on swollen hydrogels. We then succeeded to fabricate by SLA the arches with high definition using the following resins $MA_{40}POx_{66}$–PEI_4, MA_2POx_{120}, MA_2POx_{75}, and MA_2POx_{10} (Fig. 4). All the structures were subsequently washed and swollen in water for 3 days. Finally, it was also relevant to show the promising mechanical resistance of the fabricated and swollen arches by applying a maximum mass before collapsing. As illustrated in Fig. 4, the swelling rate of the fabricated arches seems to follow the same trend that was established in Fig. 4 on the fabricated cylinders $MA_{40}POx_{66}$–PEI_4 < MA_2POx_{120} < MA_2POx_{75} < MA_2POx_{10}. In correlation with the previous results, $MA_{40}POx_{66}$–PEI_4 which showed the highest degree of swelling displayed the lowest compressive resistance with the lowest mass applied, while progressively higher masses were applied on the other fabricated POx hydrogels. The highest compressive resistance was reached for the hydrogel based on MA_2POx_{10} which resists a mass of 200 g.

Moreover, to improve the resolution and the depth of light penetration in the vat photopolymerization 3D process, traditionally a low amount of a photo-absorbing dye, *i.e.* orange G is used as in our study. The dye remains chemically inert in the photopolymerization process and can therefore be removed through successive washing treatments. However, in the case of MA_2POx_{75} and MA_2POx_{10} the density of cross-linking is high and the generated network is considerably dense which results in a slow release of the dye, and consequently, a longer washing time was necessary to remove the residual amount of the dye. In contrast, after 3 days of washing, the dye was totally removed for $MA_{40}POx_{66}$–PEI_4 and MA_2POx_{120}, which is due to the much larger network with higher mesh sizes and consequently better dye diffusion.

Another proof of concept to show the potential of POx-based resin processing by SLA is presented in Fig. 5. To emphasize on the originality of the fabricated hydrogel based on polyoxazoline, the chemical abbreviation "POx" was successfully built by SLA with a layer thickness of 100 µm (Fig. 5A). The built hydrogel was then freeze dried to appreciate the porosity in SEM. As classically observed with the hydrogels, alveolar heterogeneous porosity was generated, but the layer by layer created by photo-printing remains clearly visible in the SEM picture (Fig. 5B).

Finally, a more sophisticated porous architecture was designed and built successfully with the MA_2POx_{120} precursor resin (Fig. 5C). The porous structure is a gyroid-type triply periodic minimal surface architecture as it has been already investigated in the literature for tissue engineering scaffolds[38] and considered in this study using eqn (4). Such a fabricated macroporous hydrogel retained its mechanical integrity without collapsing even at its maximum swollen state. In agreement with the water uptake measured for MA_2POx_{120} which was found to be around 570%, the volume of the gyroid porous hydrogel increased 3.5-fold regarding the initial volume just after building. The difference in the water uptake

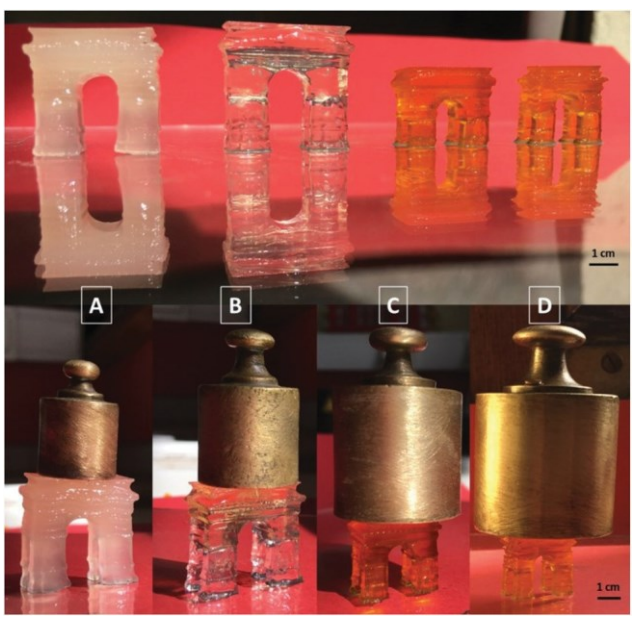

Fig. 4 Swelling in water of triumphal arch samples based on (A) $MA_{40}POx_{66}$–PEI_4, (B) MA_2POx_{120}, (C) MA_2POx_{75}, and (D) MA_2POx_{10} samples (top pictures); Samples bearing the maximum weight before distortion (A) 20 g, (B) 50 g, (C) 100 g, (D) 200 g (bottom pictures).

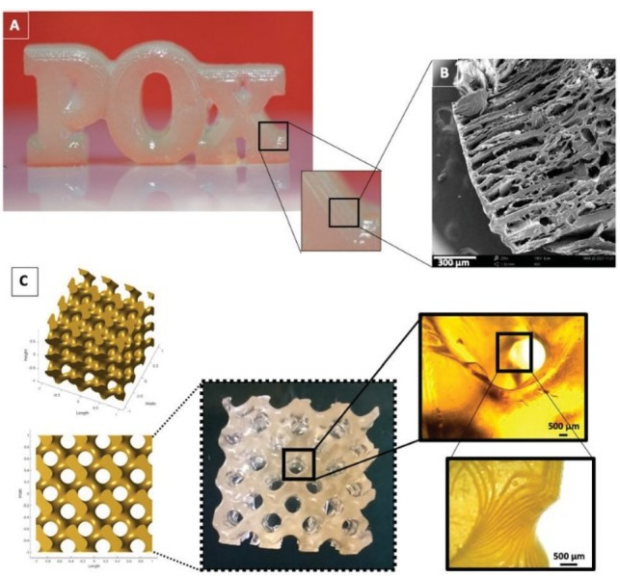

Fig. 5 (A) Building of the chemical abbreviation of polyoxazoline by SLA using MA_2POx_{120}. (B) SEM images of the freeze-dried "POx" sample that revealed layer-by-layer building by SLA. (C) From left to right, gyroid-type geometry designed by CAD software, with the resulted building by SLA using MA_2POx_{120}, and optical microscopic visualization of the built structure.

between the porous and a monolithic material could be explained by the difference in the exchange surface with water.

Cytocompatibility of the photo-sensitive POx towards the use as bioink for SLA

To examine the potential to use the photo-sensitive POx polymer as bioink by SLA, the cytocompatibility of the POx resins and POx hydrogels was investigated first in solution on the cell monolayer, and then in 3D using embedded cells. The resin precursor $MA_{40}POx_{66}$–PEI_4 was excluded from the cytocompatibility study due to i) intramolecular interactions which do not reinforce the mechanical properties, and ii) the presence of a small amount of cationic non-methacrylated cationic PEI units which could impair the cell viability.

Cytocompatibility of the POx resin precursors in solution. The metabolic activity of the different POx precursors was assessed in solution, on the L929 cell monolayer 2 days post-incubation (Fig. 6A). At a low concentration (2.5%), the result of the metabolic activity for all the polymers is similar or close to the positive control consisting of DMEM only. Increasing the concentration in solution resulted in a decrease of the cellular activity. At 5%, a decrease of approx. 18% and 25% was noted for long-chain polymers, *i.e.* MA_2POx_{75} and MA_2POx_{120} respectively. A stronger decrease of almost 50% was noted for the shorter chain MA_2POx_{10}. At 10%, MA_2POx_{75} was the less toxic polymer, but still with a decrease of 43% compared to the control (DMEM). At a higher concentration of 20%, all the polymeric solutions dramatically reduced the viability to reach values of the negative control based on the medium with 5% DMSO. The morphology of the cells corroborated the previous results. At 2.5%, the cells adhering to the plastic of the well exhibited a spreading phenotype as for the extract-free medium (Fig. S8†). In comparison, the toxic conditions stimulated by adding 5% DMSO was responsible for a decrease in cell density and a round shape morphology of all the cells (Fig. S8†). Difference in terms of cell morphology between the polymers were not detectable at 5% (Fig. S9†) but at higher concentrations of 10% and above (Fig. 6B). The short-size chain MA_2POx_{10} induced strong changes in the cell morphology (rounded cells) and a large amount of cellular debris was visible in the supernatant of the plate. The cells incubated with solutions of longer chains, *i.e.* MA_2POx_{75} and MA_2POx_{120}, exhibited a healthier morphology with cytoplasmic elongation, even though extracellular vesicles were also present surrounding the cells incubated with MA_2POx_{120}, which is also a sign of cytotoxicity. No adhering cells were present when the incubation was done with solutions at 20%, and all the cells exhibited a round-shape phenotype similar to the negative control group (data not shown). To summarize, the toxicity of those POx precursors in solution depends on their size and their concentrations. A shorter M_w induced a more pronounced toxic effect on the cells at a lower concentration. This effect can be due to the higher amount of methacrylate groups, known to be toxic when shorter polymers are used at a defined concentration compared to longer chains. At 5 up to 10%, the compatibility after 48 h of incubation of the long-chains MA_2POx_{75} and MA_2POx_{120} is still considered satisfactory.

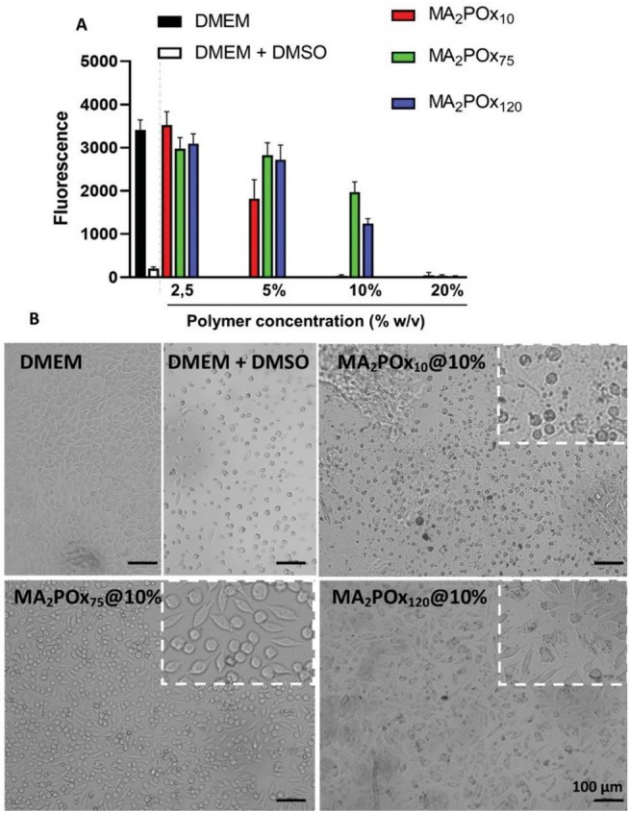

Fig. 6 Cytocompatibility of the POx in solution. (A) Metabolic activity of the L929 monolayer assessed using PrestoBlue™ cell viability reagent after 48 h of incubation with the three different POx at various concentrations. DMEM and DMEM supplemented with 5% of DMSO are used as positive and negative controls. (B) Illustration of the morphology of the L929 cells after 48 h of incubation with the different polymers at 10%.

Cytocompatibility of the POx hydrogels. Following this cytocompatibility assay of MA_2POx_n in solution, another cell type was used to test the cytocompatibility, after being encapsulated in the polymeric hydrogels. The fibroblastic cell line L929 was replaced by an immortalized cell line of human adipose derived stem cells (hASCs) as being more relevant for any tissue engineering applications. hASCs were encapsulated in hydrogels at 20 and 50% and UV-crosslinked to mimic the conditions used in SLA.

Embedding the cells in the photo-crosslinked hydrogels reveals a different threshold of cytocompatibility from when the polymers are used in solution. At 20 wt%, the hASCs remain mostly alive for the three photo-crosslinkable POx. Indeed, the percentage of viable cells is between 90 and 95% for day 3 and day 7 (Fig. 7). The good viability of the cells in the gels at 20 wt% is also shown in the fluorescence images presented in Fig. 8, after 3 and 7 days of encapsulation. Discrepancy between the MA_2POx_n appears when embedding the cells within hydrogels at higher concentration (50 wt%). In such a scenario, only the high M_w, MA_2POx_{120}, confers a compatible environment for the cells, at a similar level to when

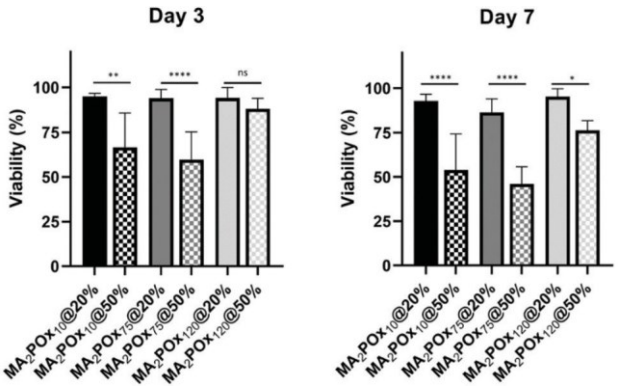

Fig. 7 Cytocompatibility study of hASCs encapsulated inside the photo-crosslinked hydrogels. Viability was assessed using Live/Dead® assay after 3 and 7 days of incubation, in hydrogels of 20 and 50%. Statistical difference was tested using ANOVA, with ns standing for "no significance", * for $p < 0.05$, ** for $p < 0.01$ and **** for $p < 0.0001$. Counting was conducted on 12 images per group.

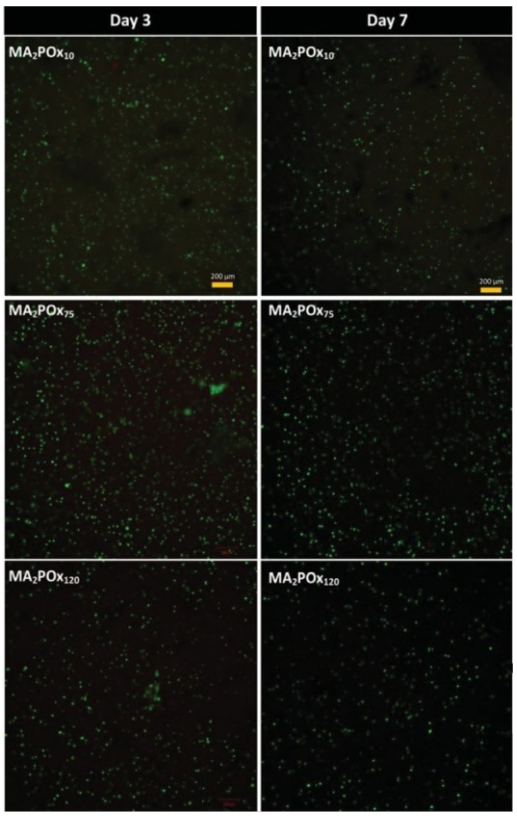

Fig. 8 Viability of the hASC cells encapsulated into the different photo-crosslinked POx hydrogels. Illustration of the Live/Dead® assay conducted after 3 and 7 days of encapsulation for the three different photopolymers.

20% of the polymer are used. The two other MA_2POx_n significantly reduced the viability of the embedded hASCs at 50%, compared to the lower concentration (20%). Incubating the samples for a longer time point (*i.e.* 7 days) revealed a similar viability trend as for day 3, with an excellent viability for the cells embedded in gels at 20%, and a satisfactory viability at a higher concentration of 50% only for long M_w MA_2POx_{120} (viability of 76%) (Fig. 7). At such a high concentration, the shorter POx and MA_2POx_{10}, chains induced a significant increase of cell death of around 50%.

In summary, the *in vitro* compatibility study performed on the three MA_2POx_n derivatives showed that the toxicity of these polymers observed in solution can be alleviated by cross-linking these chains *via* UV irradiation. Once embedded within the 3D hydrogels, an optimal cell viability is achieved by controlling the size of the POx chains, with the longer chains conferring better survival conditions than the shorter ones. The range of polymeric concentrations screened in this *in vitro* study covers the ones usually encountered for bioinks used in different additive manufacturing processes, from extrusion based bioprinting up to stereolithography, where lower (<5%) or higher (20 up to 50%) concentrations of photopolymers are required respectively.

In this original article, we have demonstrated the possibility to build by SLA a highly porous structure based on POx. The POx photopolymers represent a new class of biomaterials with great potential biomedical applications, especially in tissue reconstruction where the demand for the performant and porous hydrogel is high. The mechanical properties of POx hydrogels in its hydrated state remain remarkable and can correlate with the mechanical properties required for the reconstruction of human cartilage tissue, where the Young's modulus is around 1 MPa and the fracture strength is about 10 MPa.[6] The high water content of the POx hydrogels together with their biocompatibility are also the other important prerequisites for biomaterials to be used for instance for cartilage regeneration. We envision the future utilization of the POx photopolymers as a gel-like carrier of chondrocytes for cartilage defect repair.

Conclusions

To investigate sophisticated 3D hydrogel objects, well-defined poly(2-methyl-2-oxazoline)s were synthesized with a controlled molecular weight and sharp dispersity with various numbers of photo-sensitive units per polymer chain. The versatility of the POx chemistry was illustrated with dimethacrylated resin precursors by terminal chain functionalization as well as multimethacrylated ones after a supplementary step of partial hydrolysis of POx into POx–PEI. From these photoactive POx resins, single component hydrogels with tunable mechanical properties were successfully elaborated by SLA. This study feeds the lack of data in the literature about the mechanical properties of hydrogels based on POx. Interestingly, hydrogels own both a megapascal Young's modulus and, paradoxally, high water uptake. These compressive properties were modulated by the length of the photo-macro-crosslinker. The SLA process demonstrates promising potential for the elaboration of stiff and strong hydrogels which can find interest in the bio-

medical field of tissue engineering. The fabrication of 3D objects (*i.e.* triumphal arch) as well as sophisticated porous scaffolds with gyroid structures highlighted a high definition of the 3D printing layer-by-layer, as confirmed by SEM. The cytocompatibility study reveals that by controlling the length of the POx derivatives, and by applying a photo-crosslinking reaction, a high viability of the encapsulated cells can be maintained. These promising results provide perspectives for polyoxazoline chemistry in the challenging field of bioink formulation for the development of additive manufacturing of hydrogels in the biomedical field of tissue engineering, *e.g.* for cartilage tissue repair, where conventional hydrogels developed so far do not possess suitable mechanical properties to locally withstand the load.

Author contributions

The manuscript was written through the contributions of all authors. All authors have given approval to the final version of the manuscript.

Conflicts of interest

The authors declare no conflicts of interest.

Acknowledgements

The authors would like to acknowledge the CARTIGEN platform (IRMB, CHU, Montpellier, France) for scanning electron microscopy facilities access, especially Dr Matthieu Simon and Dr Lucas Jego for their assistance.

Notes and references

1 N. A. Peppas, P. Bures, W. Leobandung and H. Ichikawa, *Eur. J. Pharm. Biopharm.*, 2000, 50, 27–46.
2 B. V. Slaughter, S. S. Khurshid, O. Z. Fisher, A. Khademhosseini and N. A. Peppas, *Adv. Mater.*, 2009, 21, 3307–3329.
3 H. T. Peng, L. Martineau and P. N. Shek, *J. Mater. Sci. Mater. Med.*, 2007, 18, 975–986.
4 S. Van Vlierberghe, P. Dubruel and E. Schacht, *Biomacromolecules*, 2011, 12, 1387–1408.
5 N. A. Peppas, J. Z. Hilt, A. Khademhosseini and R. Langer, *Adv. Mater.*, 2006, 18, 1345–1360.
6 A. K. Means and M. A. Grunlan, *ACS Macro Lett.*, 2019, 8(6), 705–713.
7 J. L. Drury and D. J. Mooney, *Biomaterials*, 2003, 24, 4337–4351.
8 T. J. Wallin, J. Pikul and R. F. Shepherd, *Nat. Rev. Mater.*, 2018, 3, 84–100.
9 N. A. Chartrain, C. B. Williams and A. R. Whittington, *Acta Biomater.*, 2018, 74, 90–111.
10 S. B. G. Blanquer, M. Werner, M. Hannula, S. Sharifi, G. P. R. Lajoinie, D. Eglin, J. Hyttinen, A. A. Poot and D. W. Grijpma, *Biofabrication*, 2017, 9, 025001.
11 K. Arcaute, B. Mann and R. Wicker, *Acta Biomater.*, 2016, 3, 1047–1054.
12 P. Zhang, F. Sun, S. Liu and S. Jiang, *J. Controlled Release*, 2016, 244, 184–193.
13 D. G. Rudmann, J. T. Alston, J. C. Hanson and S. Heidel, *Toxicol. Pathol.*, 2013, 41, 970–983.
14 T. X. Viegas, Z. H. Fang, K. Yoon, R. Weimer and B. Dizman, Poly(oxazolines), in *Engineering of biomaterials for drug delivery systems: beyond polyethylene glycol*, Woodhead publishing series in biomaterials, ed. A. Parambath, 2018, pp. 173–198, DOI: 10.1016/b978-0-08-101750-0.00006-4.
15 M. C. Woodle, C. M. Engbers and S. Zalipsky, *Bioconjugate Chem.*, 1994, 5, 493–496.
16 Q. T. Nguyen, Y. Hwang, A. C. Chen, S. Varghese and R. L. Sah, *Biomaterials*, 2012, 33, 6682–6690.
17 T. Lorson, M. M. Lübtow, E. Wegener, M. S. Haider, S. Borova, D. Nahm, R. Jordan, M. Sokolski-Papkov, A. V. Kabanov and R. Luxenhofer, *Biomaterials*, 2018, 178, 204–280.
18 L. Simon, N. Marcotte, J. M. Devoisselle, S. Bégu and V. Lapinte, *Int. J. Pharm.*, 2020, 119536.
19 R. Hoogenboom, *Angew. Chem., Int. Ed.*, 2009, 48, 2–19.
20 M. Bauer, C. Lautenschlaeger, K. Kempe, L. Tauhardt, U. S. Schubert and D. Fischer, *Macromol. Biosci.*, 2012, 12, 986–998.
21 K. Knop, R. Hoogenboom, D. Fischer and U. S. Schubert, *Angew. Chem., Int. Ed.*, 2010, 49, 6288–6308.
22 M. Barz, R. Luxenhofer, R. Zentel and M. J. Vicent, *Polym. Chem.*, 2011, 2, 1900–1918.
23 B. Guillerm, S. Monge, V. Lapinte and J. J. Robin, *Macromol. Rapid Commun.*, 2012, 33, 1600–1612.
24 M. Glassner, M. Vergaelen and R. Hoogenboom, *Polym. Int.*, 2018, 67, 32–45.
25 G. Delaittre, *Eur. Polym. J.*, 2019, 121, 109281.
26 B. T. Benkhaled, T. Montheil, V. Lapinte and S. Monge, *J. Polym. Sci.*, 2020, 58, 2875–2886.
27 T. R. Dargaville, J. R. Park and R. Hoogenboom, *Macromol. Biosci.*, 2018, 18, 1800070.
28 M. Hartlieb, K. Kempe and U. S. Schubert, *J. Mater. Chem. B*, 2014, 3, 526–538.
29 A. Oudin, J. Chauvina, L. Gibot, M. P. Rols, S. Balord, B. Payrée, B. Lonettia, P. Vicendo, A. F. Mingotaud and V. Lapinte, *J. Mater. Chem. B*, 2019, 7, 4973–4982.
30 L. Korchia, C. Bouilhac, A. Aubert, J. J. Robin and V. Lapinte, *RSC Adv.*, 2017, 7, 42690–42698.
31 L. Korchia, C. Bouilhac, V. Lapinte, C. Travelet, R. Borsali and J. J. Robin, *Polym. Chem.*, 2015, 6, 6029–6039.
32 L. Trachsel Zenobi, M. Wong and E. M. Benetti, *Biomater. Sci.*, 2019, 2874–2886.
33 L. Hahn, M. Maier, P. Stahlhut, M. Beudert, V. Flegler, S. Forster, A. Altmann, F. Töppke, K. Fischer, S. Seiffert, B. Böttcher, T. Lühmann and R. Luxenhofer, *ACS Appl. Mater. Interfaces*, 2020, 12, 12445–12456.

34 T. Lorson, S. Jaksch, M. M. Lübtow, T. Jüngst, J. Groll, T. Lühmann and R. Luxenhofer, *Biomacromolecules*, 2017, 18, 2161–2171.
35 M. M. Lübtow, T. Lorson, T. Finger, F. K. Gröber-Becker and R. Luxenhofer, *Macromol. Chem. Phys.*, 2020, 221, 1900341.
36 C. Hu, M. S. Haider, L. Hahn, M. Yang and R. Luxenhofer, *J. Mater. Chem. B*, 2021, 9, 4535.
37 C. Hu, L. Hahn, M. Yang, A. Altmann, P. Stahlhut, J. Groll and R. Luxenhofer, *J. Mater. Sci.*, 2021, 56, 691–705.
38 S. Czich, T. Wloka, H. Rothe, J. Rost, F. Penzold, M. Kleinsteuber, M. Gottschaldt, U. S. Schubert and K. Liefeith, *Molecules*, 2020, 25, 5066.
39 S. B. G. Blanquer, M. Werner, M. Hannula, S. Sharifi, G. P. R. Lajoinie, D. Eglin, J. Hyttinen, A. A. Poot and D. W. Grijpma, *Biofabrication*, 2017, 9(2), 025001.
40 P. F. Jacobs, *J. Manuf. Syst.*, 1993, 12, 430–433.
41 X. Xu, F. A. Jerca, V. V. Jerca and R. Hoogenboom, *Adv. Funct. Mater.*, 2019, 1904886.
42 T. S. Wilems, X. Lu, Y. E. Kurosu, Z. Khan, H. Ju Lim and L. A. Smith Callahan, *J. Biomed. Mater. Res., Part A*, 2017, 105(11), 3059–3068.
43 T. X. Viegas, M. D. Bentley, J. M. Harris, Z. Fang, K. Yoon, B. Dizman, R. Weimer, A. Mero, G. Pasut and F. M. Veronese, *Bioconjugate Chem.*, 2011, 22(5), 976–986.
44 G. Morgese and E. M. Benetti, *Eur. Polym. J.*, 2017, 88, 470–485.
45 A. M. Kelly and F. Wiesbrock, *Macromol. Rapid Commun.*, 2012, 33, 1632–1647.
46 P. Šrámková, A. Zahoranová, Z. Kroneková, A. Šišková and J. Kronek, *J. Polym. Res.*, 2017, 24, 82.